ChemComm

COMMUNICATION

View Article Online
View Journal | View Issue

Cite this: *Chem. Commun.*, 2025, **61**, 941

Received 18th October 2024,
Accepted 10th December 2024

DOI: 10.1039/d4cc05558f

rsc.li/chemcomm

Isolation and characterization of a new polyoxometalate ligand, $H_3SbW_{14}O_{50}^{10-}$, and its interactions with f-elements†

Ian Colliard *[ab] and Gauthier J.-P. Deblonde *[ac]

We report the synthesis and characterization (Raman, FTIR, DLS, single crystal XRD) of $Cs_{10}H_3SbW_{14}O_{50}{\cdot}6H_2O$, which contains a new polyoxometalate building block: $H_3SbW_{14}O_{50}^{10-}$ (SbW_{14}). Solution-state fluorescence, DLS, and UV-vis absorbance results with Nd^{3+}, Eu^{3+}, Am^{3+}, and Cm^{3+} confirm that SbW_{14} acts as an efficient complexant and fluorescence sensitizer for f-elements.

Polyoxometalates (POMs) represent a large family of molecules with numerous applications, and their range of compositions and structures covers most of the periodic table.[1–3] While the POM core structures are typically built upon d-block metals[4] (W, Mo, V, Cr, Nb, Ta), their compounds often incorporate other elements and complex metal ions, and are counter-balanced by cations. POM compounds that have been characterized thus far cover over 70 elements (from hydrogen to as heavy as curium[5–8]), representing one of the most diverse class of molecules.

POMs can be seen as the inorganic equivalents of organic chelators or as an ever-expanding family of molecules that uses d-block metal octahedra (*e.g.*, WO_6^{2-}) as unitary blocks, instead of carbon–carbon bonds. POM core structures include the Lindqvist[9] (*e.g.*, $Mo_6O_{19}^{2-}$, $H_xNb_6O_{19}^{x-8}$ and $H_xTa_6O_{19}^{x-8}$), Peacock–Weakley[10] (*e.g.*, $W_5O_{18}^{6-}$), Keggin[11] (*e.g.*, $PMo_{12}O_{40}^{3-}$, $SiW_{11}O_{39}^{8-}$), Well–Dawson[12] (*e.g.*, $P_2W_{18}O_{62}^{6-}$), Anderson–Evans[13,14] (*e.g.*, $Mo_7O_{24}^{6-}$), and Preyssler[15] (*e.g.*, $P_5W_{30}O_{110}^{15-}$) ions. However, the Keggin, Wells–Dawson, and Lindqvist structures are the most widely studied.[4,15–17] For instance, in the Keggin structure ($[XW_{12}O_{40}]^{n-}$), over 25 candidates are available to be incorporated as heteroelement (X). This leads to an overwhelming number of Keggin derivatives,[18] all with potentially distinct physiochemical properties.

In this context, the subset of antimono-polytungstates (Sb-POTs), has been relatively overlooked, despite having truly unique properties. In previously reported examples of Sb-POTs, the stereoactive lone pair[19] of Sb(III) strongly influenced the structures, albeit still leading to Keggin derivatives.[20] In addition, the low charge density of Sb^{3+} shifts the POMs' stability window to slightly higher pHs, often leading to protonated Sb-POTs.[21–23] This often results in larger POMs, yet still all derived from the Keggin structure. Several Sb-POTs have been reported in the last few decades—all based on successive condensations of $[SbW_9O_{33}]^{9-}$ (SbW_9), which is a tri-lacunary Keggin ion. SbW_9 is arguably the most used Sb-POT structure and has served as precursor for larger POMs ($[NaSb_9W_{21}O_{86}]^{18-}$, $[Sb_2W_{21}O_{69}]^{6-}$, $[H_2SbW_{22}O_{76}]^{14-}$, $[Sb_8W_{36}O_{132}]^{24-}$...).[20]

In recent years, POMs have also received increasing attention for use as chelators for f-elements. In fact, POMs offer an interesting alternative relative to the more traditional organic chelators as they can act as oxygen-donor ligands but contain elements that are not easily incorporable in organic ligands. POMs can also stabilize usually unstable oxidation states of actinides, such as Am(VI).[8] The high-molecular weight of POMs also make them useful to perform microscale crystallization tests with radioisotopes.[5] In our quest to expand the chemistry of f-elements with POM ligands, we attempted to transpose our synthetic protocols recently used[5,7,24] for Keggin POMs with B^{3+}, Ga^{3+}, Si^{4+}, Ge^{4+}, and P^{5+} to antimony (Sb^{3+} – Fig. 1). Unexpectedly, the substitution of the heteroelements mentioned above for Sb^{3+} did not yield the expected Keggin POM. Not only does the behavior of antimony depart from that of the other heteroelements, but it also yielded a novel POM structure. This therefore unlocked an opportunity to explore f-element chemistry with a new type of ligand.

Herein we report the single crystal XRD structure of the POM compound $Cs_{10}H_3SbW_{14}O_{50}{\cdot}6H_2O$. This antimony(III) polytungstate is based on a new building block $[H_3SbW_{14}O_{50}]^{10-}$ (SbW_{14}). This POM was obtained by the typical synthetic route that has consistently led to Keggin-type structures with other

[a] *Physical and Life Sciences Directorate, Glenn T. Seaborg Institute, Lawrence Livermore National Laboratory, Livermore, California 94550, USA. E-mail: Colliard1@LLNL.gov, Deblonde1@LLNL.gov*
[b] *Material Sciences Division, Lawrence Livermore National Laboratory, Livermore, California 94550, USA*
[c] *Nuclear and Chemical Sciences Division, Lawrence Livermore National Laboratory, Livermore, California 94550, USA*

† Electronic supplementary information (ESI) available. CCDC 2326569. For ESI and crystallographic data in CIF or other electronic format see DOI: https://doi.org/10.1039/d4cc05558f

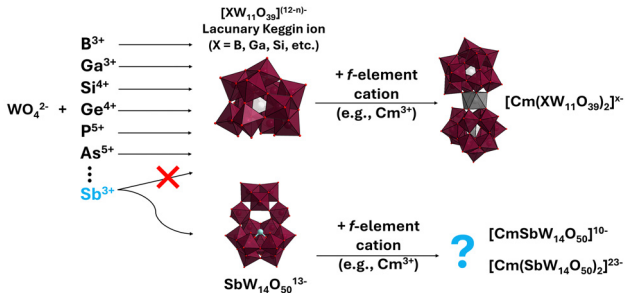

Fig. 1 Comparative synthesis scheme for the Keggin ion POM ligands and the new antimony POM reported here (unprotonated formula: $SbW_{14}O_{50}^{13-}$). While most p-block elements react with WO_4^{2-} (at pH 4–7) to form Keggin-type POMs, the same reaction with Sb^{3+} yield a different type of POM: $SbW_{14}O_{50}^{13-}$. This new POM can then be used to interact with lanthanide and actinides cations (*e.g.*, Eu^{3+}, Nd^{3+}, Am^{3+}, Cm^{3+}).

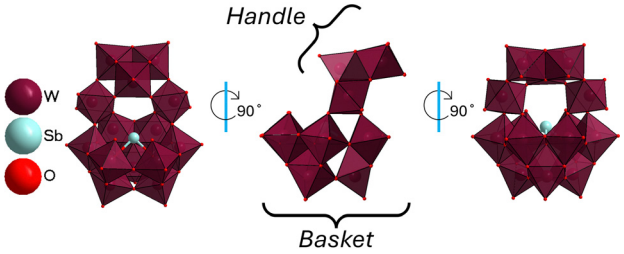

Fig. 2 Top. Structure overview of the isolated new polyoxometalate, $SbW_{14}O_{50}^{13-}$. Color code: W (maroon), O (red), Sb (cyan). Caesium and hydrogen atoms are omitted for clarity. Bottom. Raman spectra for SbW_9 and SbW_{14}.

p-block elements.[15] Additionally, we probed the potential binding of SbW_{14} to trivalent lanthanides (Eu^{3+} and Nd^{3+}) and actinides (Am^{3+} and Cm^{3+}) in solution. Eu^{3+} and Cm^{3+} were used for their fluorescence properties while Nd^{3+} and Am^{3+} were used for their absorbance properties. All four f-elements also have similar ionic radii, facilitating intercomparisons. The behavior of SbW_{14} was also contrasted with the previously known POM SbW_9. The results show that SbW_{14} can act as an effective aqueous ligand with f-elements. This represents the first study of interactions between antimony-containing ligands and heavy actinides.

SbW_{14} was obtained by conversion of the precursor $[SbW_9O_{33}]^{9-}$ (SbW_9). This precursor was synthesized as reported by Bösing *et al.*[20] without modification. The SbW_9 to SbW_{14} conversion reaction was found remarkably straightforward – happening at room temperature, ambient pressure, and in aqueous solution. From the synthesis by Bösing *et al.*, a 2 mM solution of SbW_9 was prepared (30 mg in a 100 mM acetate buffer at pH 5.5). Then, an equal volume of 6 M CsCl was added (final concentration of 3 M). After 24–48 h crystals of SbW_{14} appeared. The pH was measured at various points during the crystallization period and was stable at 5.5. For a more detailed synthesis procedure see ESI.† Single crystals of SbW_{14} were collected for structure determination, plus Raman and FTIR analysis. Fig. S1 (ESI†) clearly shows distinct Raman and FTIR features between SbW_9 and SbW_{14}.

Interestingly, the new Sb-POT could only be crystallized through the addition of caesium counterions, as opposed to pH variation. For POMs, the most conventional manner to control their speciation is by controlling the pH, to tune their hydrolysis and condensation reactions. We assume that SbW_{14} had thus far remained undiscovered because there is generally very little information in the literature about Sb-POTs with caesium counterions. This new crystal structure is unique in its synthesis, obtained through counterion-mediated reactions as opposed to pH-controlled reactions. The new structure, fully formulated as $Cs_{10}H_3SbW_{14}O_{50}{\cdot}6H_2O$, crystallizes in the orthorhombic space group $P2_12_12_1$ with a unit cell volume of 6609.5 (3) A^3; for more information see Table S1 (ESI†). One manner to describe the new Sb-POTs is as a combination of the $[SbW_9O_{33}]^{9-}$ subunit, nicknamed the 'basket', with a $[W_5(OH)_3O_{14}]^-$ 'handle' subunit (Fig. 2). The structure itself has only one symmetry element; a mirror plane along its long axis. Thus, the structure falls under the point group C_s. The 'basket' subunit, SbW_9, is the original precursor and itself is often described as the tri-lacunary version of parent Keggin structure ($[XW_{12}O_{40}]^{n-}$).[25,26] In other words, removal of three adjacent tungstates from a parent but hypothetical structure $[SbW_{12}O_{40}]^{5-}$, would results in the SbW_9 subunit. We suspect that SbW_9 does not convert to $[SbW_{12}O_{40}]^{5-}$ due to the size of Sb^{3+} and steric hindrance created by its lone electron pair. In SbW_9, six tungstates surround the central $[SbO_3]^{3-}$, with the remaining three tungstates opposite to the lone pair on Sb.

Bond valence sum calculations in SbW_{14} confirms the oxidation state at +III for Sb (Table S2, ESI†). The six surrounding tungstates can be thought of as the 'rim of the basket' while the remaining three tungstates can be the 'bottom'. The 'handle' itself, $[W_5(OH)_3O_{14}]^-$, can further be subdivided and described as a $[W_3(OH)_3O_{10}]^{5-}$ with two edge-sharing *cis*-dioxyl-tungstens, $[O{=}W{=}O]^{2+}$, binding to two of the three tungstates in the trimer. These two flanking tungstens then bind to the 'basket' completing their six-fold coordination. The 'handle' is attached to the basket *via* four out of the six tungstates surrounding Sb in the SbW_9 subunit. As a result, all tungstates have a coordination number of six, as seen for most polyoxotungstates, with rare exceptions.[27] Bond valence sum calculation on the O and W positions additionally reveal the potential location of three protons on the POMs, leading to the formula $[H_3SbW_{14}O_{50}]^{10-}$, Table S3 (ESI†).

Due to its unique composition and structure, the complexation of SbW_{14} with f-elements became of particular interest. The solution behavior of this new POT was explored through fluorescent spectroscopy (Eu^{3+} *vs.* Cm^{3+}) and UV-Visible spectrophotometry (Nd^{3+} *vs.* Am^{3+}). This represents the first study on transplutonium elements with antimony-based ligands. To first probe the physiochemical properties and complexation behavior for SbW_{14}, excitation and emission spectra were taken with Eu^{3+} at a 1 : 2 ratio (Eu^{3+} : SbW_{14}), as we expected a 1 : 1 or 1 : 2 complex based on potential binding sites of the SbW_{14} structure (Fig. 2). Excess POM to f-element was also used to ensure full complexation. Parallel experiments were done with SbW_9, for comparison purposes and to confirm that SbW_{14} does not convert back to its precursor upon binding to the

f-elements. Both SbW_9 and SbW_{14} were found to spontaneously bind to the trivalent lanthanides and actinides.

Fig. 3a and b show the normalized excitation and emission spectra, respectively for Eu^{3+} with SbW_9 and SbW_{14}. Both POMs bind to Eu^{3+} and sensitize its luminescence, but evidently *via* different pathways (Fig. 3a). The preferential excitation pathway for Eu^{3+} is *via* the POM band (λ_{ex} = 290–310 nm) in the case of SbW_{14} but *via* direct excitation of Eu^{3+} (4f–4f sharp transitions at 360–410 nm, main peak λ_{ex} = 396 nm) in the case of SbW_9. The excitation peak *via* the POM has a maximum at 343 nm for SbW_9, compared to 303 nm for SbW_{14}. When comparing the emission spectra, SbW_{14} results in more defined Eu^{3+} emission peaks, with intensities about 16-fold higher (Fig. S3, ESI†).

Lifetime dependent fluorescence further shows different complexation behaviors for SbW_9 *versus* SbW_{14} (Table S4, ESI†). While both SbW_9 and SbW_{14} yield mono-exponential decay curves with Eu^{3+} (suggesting only one type of complex(es) present), the lifetimes are significantly different, at 336 μs and 621 μs, respectively. Based on the Kimura equations,[28] which empirically correlate fluorescence lifetimes to hydration sphere, the number of coordinating water molecules decreases from three for Eu–SbW_9 to one for Eu–SbW_{14}. Although we were unable to crystallize a complex of SbW_{14} with an f-element, the solution-state fluorescence results suggest that SbW_{14} is more amenable to fulfil the f-element coordination sphere than SbW_9, leaving it less exposed to solvent molecules. Additional fluorescence titration experiments (Fig. S6–S8, ESI†), revealed that the Eu–SbW_{14} likely undergoes a gradual complexation reaction when the ratio SbW_{14} : Eu is varied. By analogy to other POMs,[4] we tentatively ascribe the observed spectral changes to the sequential formation of 1 : 1 and 1 : 2 complexes, however the precise solution-state speciation of the f-element/SbW_{14} systems will require further investigations.

When studies were extended from 4f to 5f-elements (Am^{3+} and Cm^{3+}) some deviations could be discerned in their binding behavior and physiochemical properties. Fluorescence results (Fig. 3c, d and Fig. S4, S5, ESI†) confirmed that Cm^{3+} also binds to both SbW_9 and SbW_{14}. However, contrary to Eu^{3+}, the excitation spectra revealed that, for both SbW_9 and SbW_{14}, sensitization of Cm^{3+} *via* the POM is more efficient than direct excitation. The POM excitation band is at 276 nm for Cm–SbW_9 *versus* 303 nm for Cm–SbW_{14}. Sensitization of Cm^{3+} is also more efficient *via* SbW_{14} than SbW_9, by a factor of ~4 (Fig. S4, ESI†). In other words, SbW_{14} leads to brighter complexes than SbW_9 for both Eu^{3+} and Cm^{3+}. The Cm^{3+} emission spectra are also distinct, with peak maximum at 606.0 nm for SbW_9 and 609.0 nm for SbW_{14} and an increase in intensity of a factor of 1.5. Both Cm–SbW_9 and Cm–SbW_{14} complexes exhibit a significant peak shift when compared to free Cm^{3+} under similar conditions (598.4 nm).[5] While the Kimura equation has been shown to not be applicable for most reported curium POMs,[5] apart from the simplest polytungstate $[Cm(W_5O_{18})_2]^{9-}$,[6] the time-dependent fluorescence herein is somewhat consistent with the Eu^{3+} analog (*i.e.*, lifetime longer for Cm–SbW_{14} *vs.* Cm–SbW_9). The measured lifetimes for Cm^{3+} are 133 μs for SbW_9 to 177 μs for SbW_{14} (Table S4, ESI†). This corresponds to four and three water molecules, respectively. The trend is consistent with the Eu^{3+} results and indicates a lower hydration number for the Cm–SbW_{14} complex, relative to Cm–SbW_9, but the absolute number of water molecules may not be accurate. The difference in hydration between Eu^{3+} and Cm^{3+} complexes could arise from different binding sites on SbW_{14}.

However, we posit that the Kimura equation fails to accurately describe the Cm^{3+} hydration for the Sb-POTs and starts to be less valid for Eu^{3+} as well, in this particular context. We attribute this to the alkali counterions, which are typically considered inert but have been shown to form strong ion pairs with certain POM complexes. Herein, SbW_9 uses Na^+ whereas SbW_{14} uses Cs^+, which could impact fluorescence properties. Based on the emission spectra for SbW_9, the observed species are 1 : 1 complexes, $[Eu(SbW_9O_{33})(H_2O)_3]^{6-}$ and $[Cm(SbW_9O_{33})(H_2O)_4]^{6-}$, but the speciation for Cm/Eu–SbW_{14}, remains ambiguous as we do not know its coordination mode. We also performed dynamic light scattering (DLS) experiments on SbW_{14}, and SbW_9, with and without Eu^{3+} and Cm^{3+} (Fig. S9 and Table S5, ESI†). The measured hydrodynamic diameters could support the formation of 1 : 1 complexes for both POMs under the tested conditions, although the size difference between 1 : 1 and 1 : 2 complexes may not be enough to discriminate with this technique. The role of counterions on the apparent hydrodynamic size measured by DLS also adds some uncertainty to the applicability of DLS to POM complexes.

To gain more insight into the speciation, UV-Vis absorbance experiments with Nd^{3+} and Am^{3+} were performed (Fig. 4). Both

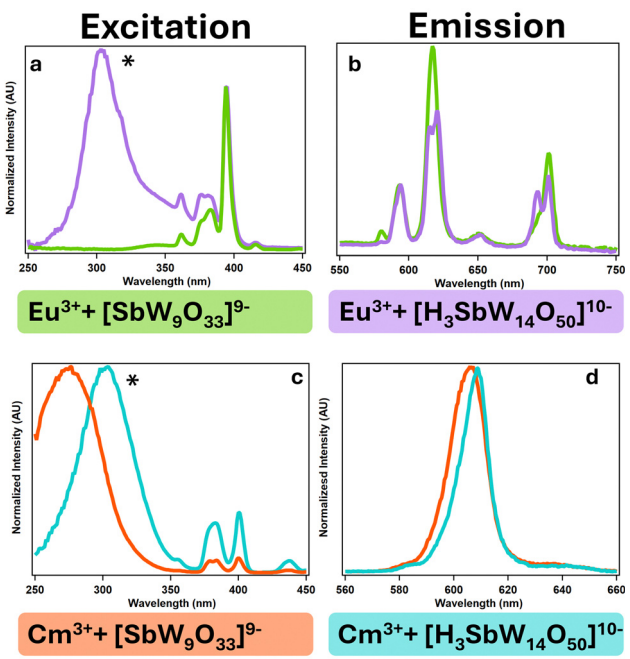

Fig. 3 Fluorescence studies on Eu–SbW_{14} (purple curves) and Cm–SbW_{14} (blue curves) compared to Eu-SbW_9 (green curves) and $CmSbW_{99}$ (orange curves). Eu^{3+} fluorescence: (a) excitation and (b) emission. Cm^{3+} fluorescence: (c) excitation and (d) emission. Fig. 3a is normalized to the excitation peak at 396 nm as Eu^{3+} sensitization *via* the POM band of SbW_9 is inefficient. See Fig. S1–S5 (ESI†) for raw intensity spectra. Solution conditions were as follows: $[Eu^{3+}]$ = 1 mM, and $[Cm^{3+}]$ = 100 μM, $[SbW_9]$ and $[SbW_{14}]$ at 2 mM and 200 μM, respectively. Sb-POTs were dissolved in 0.1 M acetate at pH of 5.5. *Indicates the POM excitation band.

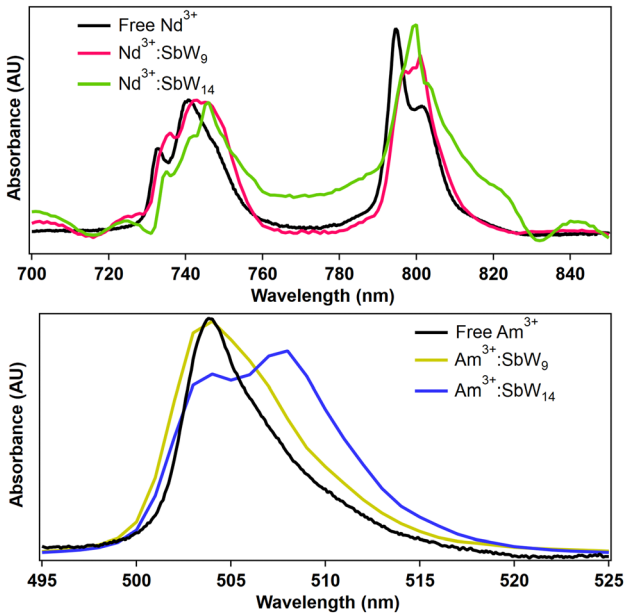

Fig. 4 UV-Vis spectra for Nd^{3+} (top) and Am^{3+} (bottom) with SbW_9 and SbW_{14}. Solution conditions: $[Nd^{3+}]$ = 1 mM. $[Am^{3+}]$ = 20 μM. $[SbW_9]$ and $[SbW_{14}]$ = 2 mM and 40 μM, respectively. Sb-POTs dissolved in 0.1 M acetate buffer (pH 5.5).

metals previously demonstrated sensitive absorbance peak shifting for different Nd^{3+}/Am^{3+}-POT species.[5,8] Am^{3+} typically exhibit significant peak shifting with the free ion absorbance at 504 nm, 1 : 1 Am^{3+} : POT complexes at 506–512 nm, and 1 : 2 complexes at 514–520 nm.[5] For both Nd^{3+} and Am^{3+}, there is evidence of complexation with both SbW_9 and SbW_{14} (Fig. 4). The absorbance bands of Nd^{3+} and Am^{3+} are both affected in the presence of SbW_9 and SbW_{14}, relative to their free ion state. In the case of Am^{3+}, SbW_9 leads to asymmetric broadening of the peak, likely indicative of a lower symmetry relative to the aqua ion. For Am^{3+} with SbW_{14}, the peak exhibits a more obvious change with a dominant peak appearing at 508.0 nm. Note that the Am^{3+}–Sb-POT experiments were limited to 20 μM concentrations, as opposed to 1 mM for Nd^{3+} or 100 μM for Cm^{3+}, which may have limited the complexation efficacy of the POMs. The results nonetheless confirm that both SbW_9 and SbW_{14} bind to trivalent lanthanides and actinides in solution. The similar extinction coefficient also supports the formation of 1 : 1 complexes under these conditions.

In conclusion, this study reports a new antimono-polytungstate structure, SbW_{14}, and its solution behavior with lanthanide and actinide elements. The $Cs_{10}H_3SbW_{14}O_{50}{\cdot}6H_2O$ structure was synthesized by an unconventional route of counterion-mediated conversion (*versus* traditional hydrolysis and condensation reactions). This compound was characterized *via* single crystal XRD, FTIR, Raman microscopy and compared to its precursor, SbW_9. Solution-state fluorescence, UV-Vis spectroscopy, and DLS experiments with Eu^{3+} *vs.* Cm^{3+}, and Nd^{3+} *vs.* Am^{3+}, revealed consistent complexation of SbW_9 and SbW_{14} to the lanthanides or actinides. Furthermore, we demonstrate that the new structure functions as a more efficient sensitizer and for both Eu^{3+} and Cm^{3+}, relative to SbW_9. Future work will focus on elucidating the solution-state speciation and expand the counterion conversion of other Sb-POTs and interactions with other f-elements.

This material is based upon work supported by the U.S. Department of Energy, Office of Science, Office of Basic Energy Sciences, Heavy Element Chemistry program at Lawrence Livermore National Laboratory under Contract DE-AC52-07NA27344. Release number: LLNL-JRNL-870910.

Data availability

The data supporting this article have been included as part of the ESI.†

Conflicts of interest

There are no conflicts to declare.

Notes and references

1 M. K. Kinnan, W. R. Creasy, L. B. Fullmer, H. L. Schreuder-Gibson and M. Nyman, *Eur. J. Inorg. Chem.*, 2014, 2361–2367.
2 J.-J. Chen, M. D. Symes and L. Cronin, *Nat. Chem.*, 2018, **10**, 1042–1047.
3 A. Gaita-Ariño, F. Luis, S. Hill and E. Coronado, *Nat. Chem.*, 2019, **11**, 301–309.
4 N. I. Gumerova and A. Rompel, *Chem. Soc. Rev.*, 2020, **49**, 7568–7601.
5 I. Colliard, J. R. I. Lee, C. A. Colla, H. E. Mason, A. M. Sawvel, M. Zavarin, M. Nyman and G. J.-P. Deblonde, *Nat. Chem.*, 2022, **14**, 1357–1366.
6 I. Colliard and G. J.-P. Deblonde, *Chem. Commun.*, 2024, **60**, 5999–6002.
7 I. Colliard and G. J.-P. Deblonde, *JACS Au*, 2024, **4**, 2503–2513.
8 H. Zhang, A. Li, K. Li, Z. Wang, X. Xu, Y. Wang, M. V. Sheridan, H.-S. Hu, C. Xu, E. V. Alekseev, Z. Zhang, P. Yan, K. Cao, Z. Chai, T. E. Albrecht-Schönzart and S. Wang, *Nature*, 2023, **616**, 482–487.
9 I. Lindqvist, *Ark. Kemi*, 1953, **5**, 247–250.
10 R. D. Peacock and T. J. R. Weakley, *J. Chem. Soc. A*, 1971, 1836–1839.
11 J. F. Keggin and W. L. Bragg, Proceedings of the Royal Society of London. Series A, Containing Papers of a Mathematical and Physical Character, 1997, **144**, 75–100.
12 B. Dawson, *Acta Crystallogr.*, 1953, **6**, 113–126.
13 J. S. Anderson, *Nature*, 1937, **140**, 850.
14 H. T. Evans, *J. Am. Chem. Soc.*, 1948, **70**, 1291–1292.
15 M. T. Pope, *Heteropoly and Isopoly Oxometalates*, Springer, Berlin, Heidelberg, 1st edn, 1983.
16 N. I. Gumerova and A. Rompel, *Sci. Adv.*, 2023, **9**, eadi0814.
17 A. Misra, K. Kozma, C. Streb and M. Nyman, *Angew. Chem., Int. Ed.*, 2020, **59**, 596–612.
18 C. A. Ohlin, *Phys. Chem. Chem. Phys.*, 2020, **22**, 4043–4050.
19 B. M. Benin, K. M. McCall, M. Wörle, D. Borgeaud, T. Vonderach, K. Sakhatskyi, S. Yakunin, D. Günther and M. V. Kovalenko, *Chem. Mater.*, 2021, **33**, 2408–2419.
20 M. Bösing, I. Loose, H. Pohlmann and B. Krebs, *Chem. – Eur. J.*, 1997, **3**, 1232–1237.
21 H. Naruke and T. Yamase, *Acta Crystallogr., Sect. C: Cryst. Struct. Commun.*, 1992, **48**, 597–599.
22 Z. Tang, M. Wang, X. Jia, S. Xie, P. Chen, D. Wang, L. Chen and J. Zhao, *Inorg. Chem.*, 2022, **61**, 14648–14661.
23 X. Xin, Y. Ma, L. Hou, Y. Wang, X. Xue, J. Lin and Z. Han, *Inorg. Chem.*, 2019, **58**, 9567–9571.
24 I. Colliard and G. J.-P. Deblonde, *Inorg. Chem.*, 2024, **63**, 16293–16303.
25 J. F. Keggin, Proceedings of the Royal Society of London. Series A, Containing Papers of a Mathematical and Physical Character, 1934, **144**, 75–100.
26 C. Falaise, G. Mpacko Priso, N. Leclerc, M. Haouas and E. Cadot, *Inorg. Chem.*, 2023, **62**, 2494–2502.
27 G. Deblonde and I. Colliard, *Acta Crystallogr., Sect. E: Struct. Rep. Online*, 2024, **80**, 667–670.
28 T. Kimura, G. R. Choppin, Y. Kato and Z. Yoshida, *Radiochim. Acta*, 1996, **72**, 61–64.

